Dynamic Reduced Normalized Gaussian Network Method for Topology Optimization of Electromagnetic Devices

Xiaohan Kong[1], Kantapat Tonchua[2], Pirat Khunkitti[2], and Hajime Igarashi[3]
[1]Graduate School of Engineering, Kyoto University, Kyoto 615-8530, Japan
[2]Department of Electrical Engineering, Faculty of Engineering, Khon Kaen University, Khon Kaen, Thailand
[3]Data-Driven Interdisciplinary Research Emergence Department (D-RED), Hokkaido University, Sapporo, Japan

This paper proposes an efficient method to represent topology using fewer variables by combining the normalized Gaussian network with a truncated eigendecomposition. In this method, new orthogonal basis functions are derived from the original Gaussian functions, allowing the main features of the topology to be captured compactly. Since the bases are orthogonal after decomposition, we also introduce a strategy to dynamically increase the number of basis functions during optimization, ensuring that each newly added basis does not interfere with the existing ones. By progressively adding bases, the topology evolves from a coarse representation to a more refined structure, which helps reduce optimization time and avoid getting trapped in poor local solutions.

***Index Terms*—Topology optimization, Gaussian basis functions, eigendecomposition.**

I. Introduction

TOPOLOGY OPTIMIZATION (TO) [1], [2] has been widely used to design novel structures beyond conventional parameter optimization, contributing significantly to the improvement of electromagnetic device performance. TO methods can be broadly classified into two categories: gradient-based and stochastic (or gradient-free) methods. Gradient-based methods, such as the level-set [3] and density-based [4] formulations, offer fast convergence and can handle a large number of design variables efficiently. However, they often face difficulties in nonlinear or non-differentiable problems and are prone to local minima.

Stochastic methods, such as the ON/OFF method [3], treat each element's material state as a discrete variable evolved by stochastic algorithms such as evolutionary strategies. These gradient-free approaches offer strong global search capability but become inefficient as the number of design variables increases. To reduce variables and obtain smoother topologies, the material distribution is represented as a weighted sum of basis functions [4], [5]. The normalized Gaussian network (NGnet) [5], which employs Gaussian basis functions, has demonstrated robust performance in electromagnetic design [6].As an extension of NGnet, the kernel ridge regression (KRR) formulation [7] enhances the representational flexibility of the material field, yet still relies on a fixed and high-dimensional set of bases, which often leads to small spurious features. To address the dimensionality issue, Luo [8] proposed the material-field series-expansion (MFSE) method, which applies eigendecomposition of the Gaussian kernel to construct reduced basis functions in a density-based framework. Although this approach effectively decreases the number of variables, it still retains several hundred variables after reduction and relies on gradient-based optimization, limiting its global search capability and flexibility.

Corresponding author: Xiaohan Kong (email: kongxiaohan.em@gmail.com).

Inspired by this idea, we incorporate eigendecomposition into the NGnet framework and propose the reduced NGnet method, which approximates the NG bases by truncating the kernel matrix and retaining only the dominant modes. Furthermore, the dynamic reduced NGnet (DR-NGnet) method begins with a very low-dimensional basis and gradually increases the number of bases during optimization. This dynamic stochastic framework maintains the efficiency and the global search ability of NGnet. Two strategies for dimensional expansion are considered: a fixed-schedule strategy and a convergence-based adaptive strategy. This dynamic framework makes the optimization move smoothly from coarse to fine, keeping a good balance between efficiency and result quality while avoiding early convergence.

II. Method

A. Reduced NGnet representation

In the conventional NGnet method, we define the shape function $y(\boldsymbol{x})$ as a linear combination of NG basis functions:

$$y(\boldsymbol{x}) = \sum_{i=1}^{N} w_i \, g_i(\boldsymbol{x}, \boldsymbol{u}_i), \tag{1}$$

where the parameters are defined as follows:

- N: number of NG bases;
- $w_i \in [-1, 1]$: weight coefficient of the i-th NG basis;
- d: spatial dimension (e.g., 2D or 3D);
- $\boldsymbol{x} \in \mathbb{R}^d$: sampling point position vector;
- $\boldsymbol{u}_i \in \mathbb{R}^d$: center of the i-th NG basis.

Each NG basis function $g_i(\boldsymbol{x}, \boldsymbol{u}_i)$ is computed by normalizing the original Gaussian function over all basis centers, ensuring that the sum of all basis functions equals one at each point $\boldsymbol{x}$:

$$g_i(\boldsymbol{x}, \boldsymbol{u}_i) = \frac{G(\boldsymbol{x}, \boldsymbol{u}_i)}{\sum_{j=1}^{N} G(\boldsymbol{x}, \boldsymbol{u}_j)}, \tag{2}$$

where the original Gaussian function $G(\boldsymbol{x}, \boldsymbol{u}_i)$ is given by:

$$G(\boldsymbol{x}, \boldsymbol{u}_i) = \frac{1}{(2\pi\sigma^2)^{d/2}} \exp\left(-\frac{1}{2\sigma^2}\|\boldsymbol{x} - \boldsymbol{u}_i\|^2\right), \tag{3}$$

where σ denotes the standard deviation of the Gaussian, and $\|\cdot\|$ represents the Euclidean norm.

Each element $\boldsymbol{x_e}$ is assigned a material by the sign of $y(\boldsymbol{x_e})$, where positive and negative values indicate different materials:

$$M_e = \begin{cases} \text{material 1} & (y(\boldsymbol{x_e}) \geq 0) \\ \text{material 2} & (y(\boldsymbol{x_e}) < 0). \end{cases} \tag{4}$$

For a more compact formulation, we define the vector of NG basis functions at point $\boldsymbol{x}$ as:

$$\boldsymbol{k}(\boldsymbol{x}) = \begin{bmatrix} k_1(\boldsymbol{x}), & k_2(\boldsymbol{x}), & \ldots, & k_N(\boldsymbol{x}) \end{bmatrix}^T, \tag{5}$$

where $k_i(\boldsymbol{x}) = g_i(\boldsymbol{x}, \boldsymbol{u}_i)$, and the weight vector is defined as:

$$\boldsymbol{w} = \begin{bmatrix} w_1, & w_2, & \ldots, & w_N \end{bmatrix}^T. \tag{6}$$

Then the shape function can be written as an inner product:

$$y(\boldsymbol{x}) = \boldsymbol{k}(\boldsymbol{x})^T \boldsymbol{w}. \tag{7}$$

For n sampling points $\boldsymbol{x}_1, \boldsymbol{x}_2, \ldots, \boldsymbol{x}_n$, we construct the basis matrix:

$$\hat{\boldsymbol{G}} = \begin{bmatrix} k_1(\boldsymbol{x}_1) & \ldots & k_N(\boldsymbol{x}_1) \\ k_1(\boldsymbol{x}_2) & \ldots & k_N(\boldsymbol{x}_2) \\ \vdots & & \vdots \\ k_1(\boldsymbol{x}_n) & \ldots & k_N(\boldsymbol{x}_n) \end{bmatrix} \in \mathbb{R}^{n \times N}, \tag{8}$$

so that the vector of shape function values at all sampling points can be expressed as:

$$\boldsymbol{y} = \hat{\boldsymbol{G}} \boldsymbol{w}. \tag{9}$$

To further reduce the dimensionality and extract the most significant modes, we construct the kernel matrix:

$$\boldsymbol{K} = \hat{\boldsymbol{G}}^T \hat{\boldsymbol{G}} \in \mathbb{R}^{N \times N}, \tag{10}$$

which is symmetric and positive semi-definite.

We then perform eigendecomposition of $\boldsymbol{K}$ to construct a set of orthogonal basis functions:

$$\boldsymbol{K} = \boldsymbol{V} \boldsymbol{\Lambda} \boldsymbol{V}^T, \tag{11}$$

where $\boldsymbol{\Lambda} = \text{diag}(\lambda_1, \ldots, \lambda_N)$ contains the eigenvalues sorted in descending order, and $\boldsymbol{V} = [\boldsymbol{v}_1, \ldots, \boldsymbol{v}_N]$ are the corresponding orthonormal eigenvectors. To construct a set of reduced basis function, we select the first m dominant modes:

$$\boldsymbol{\Lambda}_m = \text{diag}(\lambda_1, \ldots, \lambda_m), \tag{12}$$

$$\boldsymbol{V}_m = \begin{bmatrix} \boldsymbol{v}_1, & \ldots, & \boldsymbol{v}_m \end{bmatrix}. \tag{13}$$

Then the shape function can be expressed as:

$$y(\boldsymbol{x}) \approx \hat{\boldsymbol{G}} \boldsymbol{V}_m \boldsymbol{\Lambda}_m^{1/2} \boldsymbol{V}_m^T \boldsymbol{w}, \tag{14}$$

or equivalently:

$$y(\boldsymbol{x}) \approx \sum_{i=1}^{m} c_i \, \varphi_i(\boldsymbol{x}), \quad (m \leq N) \tag{15}$$

where

$$\varphi_i(\boldsymbol{x}) \approx \sum_{j=1}^{N} k_j(\boldsymbol{x}) V_{ij}. \tag{16}$$

Here, $\varphi_i(\boldsymbol{x})$ defines the i-th orthogonal basis function (hereafter referred to as an "orthogonal basis" to distinguish it from the original NG basis), and V_{ij} represents the i-th component of the j-th eigenvector, i.e., $V_{ij} = [\boldsymbol{v}_i]_j$. The coefficients c_i are the weights corresponding to the orthogonal bases $\varphi_i(\boldsymbol{x})$, and these weights are treated as the optimization variables, each taking values in the range $[-1, 1]$. When selecting the first m bases, only m optimization variables are required, reducing the dimensionality compared to the full space of N variables.

In a 100×100 mm square region, 100 NG bases with $\sigma = 7$ mm are uniformly distributed. Here, these parameter settings are chosen simply to illustrate the effectiveness of the proposed method. Then, 100 orthogonal bases are obtained by performing eigendecomposition of the kernel matrix. Fig. 1 shows the eigenvalues in descending order, where the dominant modes capture most of the variance. Fig. 2 illustrates the first and last five orthogonal bases, corresponding to the largest and smallest eigenvalues. The dominant modes exhibit smooth, global patterns, while the higher-order modes capture localized, oscillatory details. Fig. 3 compares topology representations using different numbers of retained orthogonal bases m. Larger m includes more fine details, whereas smaller m emphasizes global features. If this property is utilized during optimization by dynamically adjusting m to evolve the topology from coarse to fine, it can simplify the optimization problem and improve convergence.

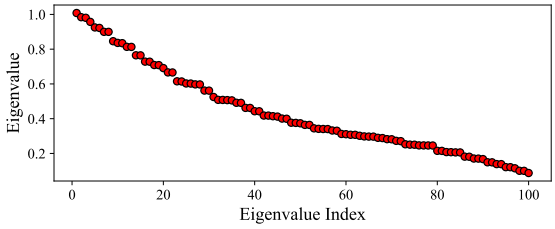

Fig. 1: Eigenvalues sorted in descending order.

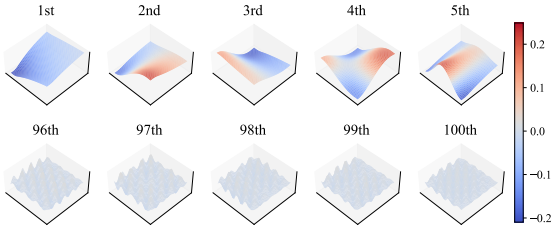

Fig. 2: Top five and last five dominant reduced orthogonal basis functions.

Fig. 3: Topologies under different orthogonal bases.

B. Dynamic reduced NGnet method

The reduced NGnet basis functions (orthogonal bases) have the potential to reduce the dimensionality in optimization. We refer to this method, which optimizes using a fixed m, as the reduced NGnet method (R-NGnet). The optimal dimension m depends on the complexity of the specific optimization problem: too small m may result in insufficient representation and convergence to a local optimum, whereas too large m diminishes the benefits of dimensionality reduction. Therefore, it is challenging to determine a fixed m that balances optimization speed and quality.

To address this issue, we propose dynamically increasing the number of retained bases m during optimization, starting from a coarse, low-dimensional space and progressively refining in a higher-dimensional one. We refer to this approach as DR-NGnet. Formally, the optimization starts with an initial dimension m_0. At certain generations, the dimension m is increased by Δm through the addition of new bases:

$$m(g) = \begin{cases} m(g-1) + \Delta m, & \text{if } g \in G_{\text{extend}}, \\ m(g-1), & \text{otherwise.} \end{cases} \tag{17}$$

where g denotes the generation index, and G_{extend} represents the set of generations where the dimension is increased.

We employ the Covariance Matrix Adaptation Evolution Strategy (CMA-ES) to perform the optimization. CMA-ES has been widely recognized for its global search ability in multimodal and non-convex optimization problems, due to its adaptive covariance update and cumulative step-size adaptation [9], which makes it suitable for solving TO problems. Fig. 4 illustrates the dimension expansion process, where the red points indicate the newly added individuals. The yellow dashed circle represents the sampling range in the current generation (m dimensions). After expanding by Δm, the red ellipse denotes the sampling range in the $m+\Delta m$ dimensional space. Red star-shaped points indicate the newly added individuals, while black ones correspond to the previous individuals.

The distribution of the individuals in the next generation is governed by the CMA-ES covariance matrix $\boldsymbol{C}$, which is accordingly extended as:

$$\boldsymbol{C}^{(m+\Delta m)} = \begin{bmatrix} \boldsymbol{C}^{(m)} & 0 \\ 0 & \boldsymbol{I} \end{bmatrix}, \tag{18}$$

where $\boldsymbol{C}^{(m)} \in \mathbb{R}^{m\times m}$ is the current covariance matrix, and $\boldsymbol{I} \in \mathbb{R}^{\Delta m\times \Delta m}$ is the identity matrix, with ones on the diagonal and zeros elsewhere. A scaling factor can be applied to $\boldsymbol{I}$ to adjust the initial covariance of the new dimensions.

After the covariance extension, the new individuals are sampled according to the updated covariance matrix $\boldsymbol{C}$, with small random perturbations:

$$x_{\text{new}} \sim \mathcal{N}\big(0,\ (0.1\,\sigma_s)^2\big), \tag{19}$$

where σ_s denotes the current global step-size of CMA-ES. The perturbation is approximately 10% of the current value of σ_s, though this value can be adjusted depending on the problem.

Deciding when to expand the dimensionality is an important issue. We evaluate two strategies: a fixed schedule, which increases the number of modes at fixed iteration intervals, and an adaptive schedule, which responds to the convergence of the objective. Fig. 5 illustrates two different strategies. In the fixed schedule strategy, the dimension is increased by Δm after every fixed interval of Δg generations. In contrast, the adaptive schedule triggers the expansion by Δm only when the improvement rate of the best objective value over the past five generations falls below ε. In both strategies, the maximum dimension is constrained by the total number of NG bases before reduction, N, which we refer to as the full dimension.

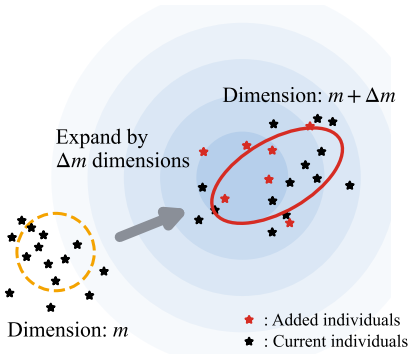

Fig. 4: Dynamic dimensionality expansion.

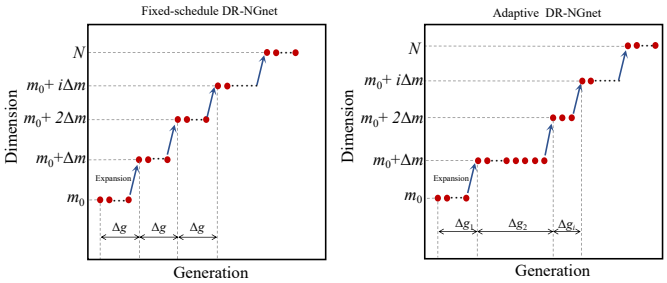

Fig. 5: Two different strategies for dimension expansion.

The strategy for the adaptive schedule of the DR-NGnet method is shown in Fig. 6. Notably, we use the percentage decrease of the best objective value over the most recent five generations as the criterion:

$$\text{mean}\big(\Delta f_{g-4:g}\big) < \varepsilon, \tag{20}$$

where g denotes the generation index. When this value falls below a predefined threshold, a dimension expansion is triggered. In the following tests, we set this threshold to 10%. However, after each expansion, a 3-generation cooling-down buffer of generations is imposed to allow the new dimensions time to evolve, preventing the next expansion from being triggered before the added dimensions can take effect.

The feasibility of this dynamic scheme relies on the orthogonality of the reduced basis functions. Under the discrete inner product defined on the sampling points, the reduced modes satisfy

$$\langle \varphi_i,\ \varphi_j \rangle = 0 \quad (i \neq j), \tag{21}$$

which ensures that newly added modes do not overlap with the already-optimized ones. As a result, the optimization can

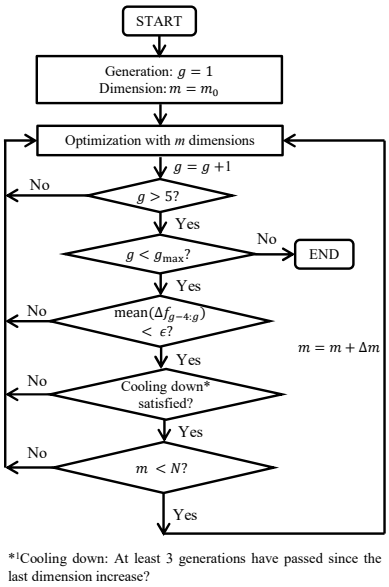

*[1]Cooling down: At least 3 generations have passed since the last dimension increase?

Fig. 6: Flowchart of the DR-NGnet method with adaptive dimension expansion.

continue smoothly after each dimension expansion without disturbing the previously explored search directions. In the conventional NGnet method, dynamic dimension extension requires reconfiguring the distribution and sizes of the NG bases at each expansion step. This can disrupt the continuity of the topology. Moreover, the exploration history in the lower-dimensional space cannot be effectively carried over to the new higher-dimensional space. Therefore, the ability to perform dynamic dimension expansion is a unique advantage of the reduced NGnet method.

III. Optimization Results

A. Optimization problem: shield problem

A magnetic shield problem as shown in Fig. 7a is used to test the proposed method. The 2D geometry in the xy-plane is axisymmetric about the y-axis and also mirror-symmetric about the horizontal midline (x-axis). The objective is to determine shield shapes that minimize the magnetic energy in the target region while using the smallest shield iron:

$$f = \frac{E}{E_{ref}} + \frac{S}{S_{ref}}, \tag{22}$$

where E is the magnetic energy in the target region, and S is the area of the shielding iron. $E_{\mathrm{ref}} = 1$ nJ and $S_{\mathrm{ref}} = 29$ cm^2 are normalized constants. 96 NG bases are uniformly deployed in the design region, and $\sigma = 7$ mm. Here, $\sigma = 7$ mm is the standard deviation of the NG basis function, defining the spatial extent of its significant influence. The circle with a radius of 7 mm in Fig. 7 illustrates this effective range. The number of 96 NG bases is empirically determined as a balance between shape diversity and optimization complexity; using more NG bases could lead to higher computational difficulty. The B-H characteristics of the material used for shield modeling are shown in Fig. 7b. The E value for each topology was evaluated using the finite element method (FEM), with the number of mesh elements typically ranging from 7,000 to 10,000.

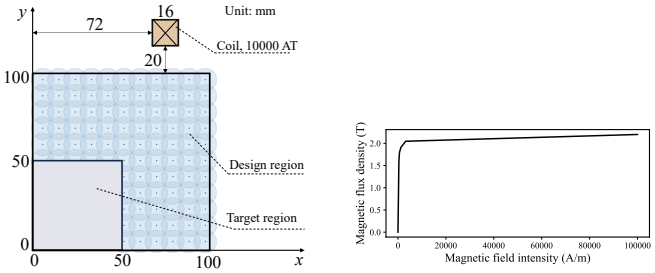

(a) Magnetic shield problem. (b) B-H curve.

Fig. 7: Design model and the B-H curve of the shield material.

B. DR-NGnet method with fixed schedule

We compared the optimization performance of the traditional NGnet method and the proposed DR-NGnet method with a fixed expansion schedule. For the DR-NGnet method, we used 96 uniformly distributed NG basis functions as shown in the left panel of Fig. 8. The initial dimension m_0 is set to 16 and is extended by $\Delta m = 5$ every two generations until it reaches the total number of bases, 96. For the traditional NGnet method, we performed optimization using both 96 and 21 NG bases, as shown in Fig. 8. The choice of 21 NG bases was intended to demonstrate the optimization performance of the conventional NGnet method when using a similarly small number of variables as in the DR-NGnet method. Since it is not possible to continuously vary the number of NG bases while covering the entire design domain, we selected 21 basis functions for comparison. For all three methods, we employ CMA-ES to solve the shield problem, evaluating 17 candidate solutions at each iteration and performing 5 independent runs, each with 100 iterations.

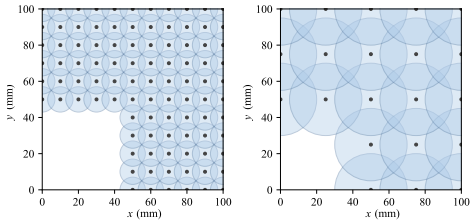

Fig. 8: Two base settings: (a) 96 NG bases ($\sigma = 7$ mm); (b) 21 NG bases ($\sigma = 15$ mm).

Fig. 9 compares the evolution histories of the traditional NGnet and the proposed DR-NGnet methods. The DR-NGnet, starting from a lower dimension ($m_0 = 16$) than the 96-basis NGnet, shows a faster initial decrease in the objective function and earlier convergence in all five runs. The 21-basis NGnet also converges quickly at first due to its lower dimensionality, but two of the five runs get trapped in local optima. Fig. 10 illustrates the worst-case topologies of the three methods. In their worst cases, both the 96D traditional NGnet and the DR-NGnet converged to a two-layer shielding structure, whereas

the 21D traditional NGnet converged to a local optimum, a single-layer structure, which fails to fully shield the target region and results in higher magnetic energy.

Fig. 11a and Fig. 11b show the evolution of the best topologies of each generation for the DR-NGnet with fixed schedule and NGnet methods, respectively. We only present the iteration process up to the 40th generation, since beyond this point both methods mainly perform local refinements on the two-layer shielding structure without significant changes. DR-NGnet starts with a simple structure and adds details as the dimension increases, while NGnet produces a complex structure from the beginning.

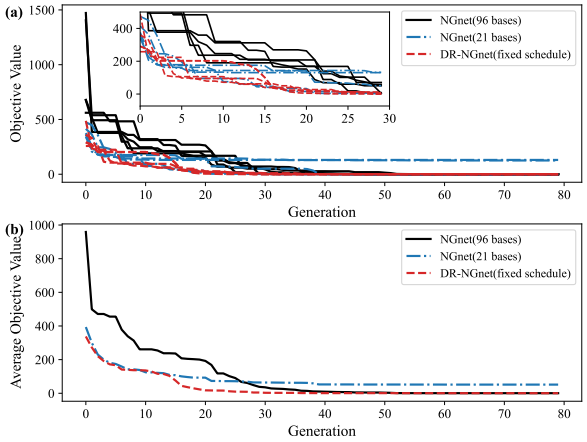

Fig. 9: Optimization histories of the DR-NGnet (fixed schedule) and NGnet methods: (a) all five runs; (b) average histories.

Fig. 10: Comparison of worst-case optimal topologies between the DR-NGnet (fixed schedule) and NGnet methods.

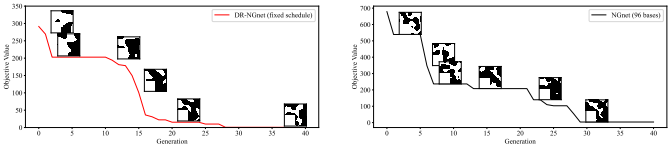

(a) DR-NGnet (fixed schedule) (b) NGnet (96 bases)

Fig. 11: Evolution of the topology during the optimization process using the DR-NGnet (fixed schedule) and NGnet (96 bases) methods.

Since different fixed schedules can influence the optimization process, we compared the optimization results starting from dimensions of 8, 16, and 32, respectively, against the R-NGnet method with the corresponding fixed dimensions of 8, 16, and 32, as shown in Fig. 12. The generations at which the dimensions are expanded are indicated by gray dashed lines. The R-NGnet method with constant dimensions of 8 and 16

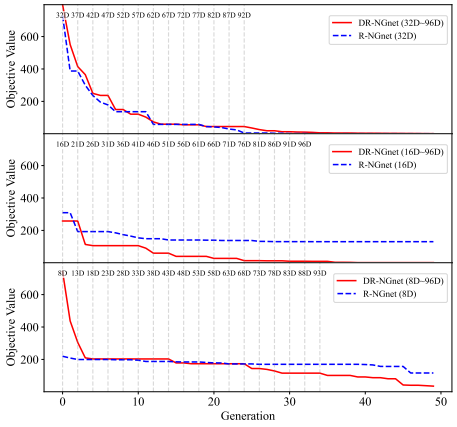

Fig. 12: Comparison of optimization histories between the DR-NGnet (fixed schedule, and start at 32D, 16D, and 8D) and R-NGnet (32D, 16D, and 8D).

tends to get trapped in local optima, whereas the DR-NGnet method mitigates this risk. Furthermore, the objective value typically decreases after the dimension expansion. Compared to the traditional NGnet method at both high (96D) and low (21D) dimensions, the DR-NGnet method strikes a better balance between optimization efficiency and performance. Its fast convergence is enabled by the smaller initial search space, while periodic dimension expansion helps avoid local optima.

Nevertheless, in the fixed-dimension expansion approach, the timing of the dimension increase is determined a priori by the user, which might not always be optimal or reliable under varying conditions. Therefore, in the next section, we will discuss the results from the adaptive dimension expansion strategy.

C. DR-NGnet method with adaptive schedule

This section evaluates the optimization performance of the adaptive dimension-expansion DR-NGnet method. An initial dimension of $m_0 = 8$ is used, and it is increased by $\Delta m = 5$ upon each expansion, until reaching the maximum dimension of 96. Fig. 13 compares the conventional NGnet method with the DR-NGnet method using fixed and adaptive schedules. The red and purple lines represent the fixed and adaptive cases, respectively. Both schedules converged faster than the conventional NGnet. The DR-NGnet with fixed and adaptive schedules reached $f \leq 1$ at the 39th and 44th generations on average, respectively, compared with 53rd generations for NGnet, corresponding to about 26% and 17% reductions in optimization time. However, the fixed schedule requires careful tuning of m, which may vary by problem. For instance, the result here was obtained with $m = 32$, while smaller values ($m = 16$ or $m = 8$, shown as blue lines in Fig. 12) led to local optima. The adaptive schedule avoids this issue by starting from $m = 8$ and increasing the dimension adaptively. Hence, the adaptive schedule is more practical and reliable. Fig. 14 shows the dimension expansion timings in three random tests under the same settings. When the objective value decreases slowly, expansion is triggered to avoid local optima. The

three independent optimizations used the same parameters but reached similar optimal solutions through different search paths, reflecting the stochastic nature of CMA-ES and the robustness of the proposed method.

Fig. 15 compares the best topologies up to the 80th generation for five runs of the DR-NGnet (adaptive schedule) and NGnet methods. DR-NGnet more effectively captured the two-layer structure and achieved a lower average objective value.

Fig. 16a and Fig. 16b show the topology evolution during optimization for the DR-NGnet (adaptive schedule) and R-NGnet (16 bases) methods, respectively. Both methods encountered the same local optimum with an objective value around 150 during the process; however, the DR-NGnet escaped it through aggressive dimension expansion, while the R-NGnet (16 bases) remained trapped.

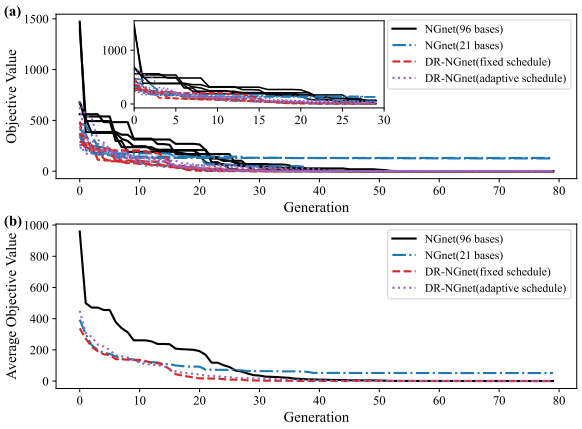

Fig. 13: Comparison of optimization results for the DR-NGnet (fixed/adaptive) and NGnet methods: (a) histories of all five runs; (b) average histories.

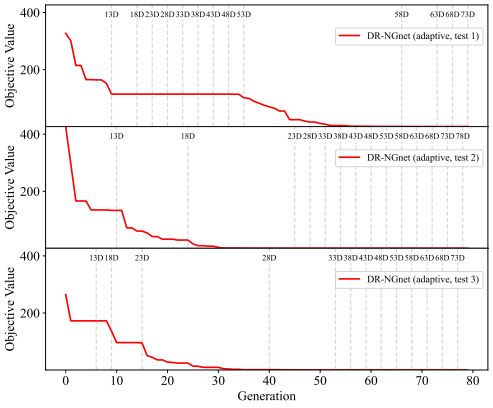

Fig. 14: Adaptive DR-NGnet optimization histories for three test cases, with gray lines indicating dimension expansion.

IV. Conclusion

We introduced a reduced NGnet method for TO, where orthogonal basis functions are obtained through truncated eigendecomposition of the kernel matrix. On this basis, we proposed the DR-NGnet method with dynamic dimension expansion and

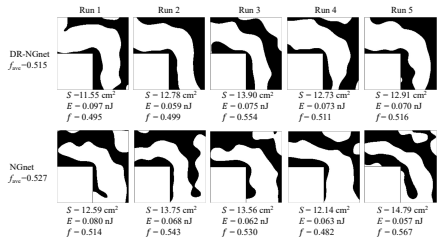

Fig. 15: Comparison of optimal topologies between the DR-NGnet (adaptive schedule) and NGnet methods.

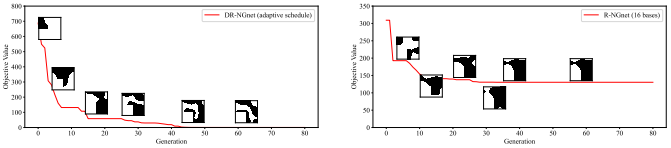

(a) DR-NGnet (adaptive) (b) R-NGnet (16 bases)

Fig. 16: Evolution of the topology during the optimization process using the DR-NGnet (adaptive schedule) and R-NGnet (16 bases) methods.

tested two strategies: fixed schedule and adaptive schedule. The results show that DR-NGnet enables the topology to evolve from coarse to fine, accelerates convergence, and helps avoid local optima. Future work will focus on extending this method to more complex problems, such as multi-material, three-dimensional, and motor optimizations.

Acknowledgment

This work was supported by the Japan Society for the Promotion of Science (JSPS) Research Fellowships for Young Scientists under Grant 24KJ0270.

References

[1] Y. Li, S. Yang, and Z. Ren, "A multi-objective topology optimization methodology using deep learning and its application to electromagnetic devices," *IEEE Transactions on Magnetics*, vol. 60, no. 3, pp. 1–5, Mar. 2024.

[2] H. Igarashi, *Topology Optimization and AI-based Design of Power Electronic and Electric Devices*. Academic Press, 2024.

[3] C. Midha, M. H. Mohammadi, R. C. P. Silva, and D. A. Lowther, "Selection of spatial filters for on/off based topology optimization of a c-core electromagnetic actuator," *IEEE Transactions on Magnetics*, vol. 55, no. 10, pp. 1–4, Oct. 2019.

[4] T. Tsuji and K. Hirayama, "Design of optical circuit devices using topology optimization method with function-expansion-based refractive index distribution," *IEEE Photonics Technology Letters*, vol. 20, no. 12, pp. 982–984, Jun. 2008.

[5] T. Sato, K. Watanabe, and H. Igarashi, "Multimaterial topology optimization of electric machines based on normalized gaussian network," *IEEE Transactions on Magnetics*, vol. 51, no. 3, pp. 1–4, Mar. 2015.

[6] Z. Sun, H. Otsuki, T. Sato, and K. Watanabe, "Topology optimization of a switched reluctance machine by electromagnetic-structural multiphysics finite element analysis," *IEEE Transactions on Magnetics*, vol. 60, no. 3, pp. 1–5, Mar. 2024.

[7] T. Sato, K. Watanabe, and H. Igarashi, "A topology optimization of electromagnetic devices based on kernel ridge regression as a variant of gaussian network-based shape representation," *IEEE Transactions on Magnetics*, vol. 60, no. 12, pp. 1–5, Dec. 2024.

[8] Y. Luo and J. Bao, "A material-field series-expansion method for topology optimization of continuum structures," *Computers and Structures*, vol. 225, p. 106122, Dec. 2019.

[9] N. Hansen, "The cma evolution strategy: A comparing review," in *Towards a New Evolutionary Computation*. Springer, 2006, pp. 75–102.